Advanced Steel Construction – Vol. 20 No. 4 (2024) 406–412
DOI:10.18057/IJASC.2024.20.4.8

EXPERIMENTAL AND NUMERICAL ANALYSIS ON THE MECHANICAL BEHAVIOR OF A GLULAM SUSPENDOME

Chen-Rui Zhang [1], Jian-Xiong Zhao [2, *], Hong-Bo Liu [2, 3], Shi-Xing Zhao [4], Jing-Xian Zhao [2], Shu-Heng Yang [4] and Ting Zhou [2]

[1] *School of Civil Engineering, The University of Sydney, Sydney, Australia*
[2] *Department of Civil Engineering, Tianjin University, Tianjin 300072, China*
[3] *Department of Civil Engineering, Hebei University of Engineering, Handan 056000, China*
[4] *Sichuan Provincial Architectural Design and Research Institute Co., Ltd., Chengdu, Sichuan 610000, China*
** (Corresponding author: E-mail: zhao_jx@tju.edu.cn)*

ABSTRACT

To enhance the overall stability of the glulam reticulated shell, an innovative structural solution, the glulam suspendome, is introduced by integrating a cable-strut system. A destructive test utilizing 13 hydraulic jacks was carried out to assess the overall stability. This study primarily encompassed analyses of load-displacement curves for nodes, load-strain characteristics of structural members, load-cable force assessments of hoop cables, and an investigation into failure mode. The failure mode of the structure involved instability around the weak axis of the member near the mid-span node, along with member fracture. The structure sustained an ultimate load of 1094.21kN (84.17kN×13). Based on the parameter analysis of the finite element model (FEM) of more than 200 cases of glulam suspendome, the ultimate bearing capacity improvement coefficient (k) of the suspendome structure compared with single-layer reticulated shell was given. The experimental and numerical analysis on the mechanical properties of glulam suspendome serves as a dependable point of reference for the design of other glulam suspendome.

ARTICLE HISTORY

Received: 6 January 2024
Revised: 27 June 2024
Accepted: 30 August 2024

KEYWORDS

Glulam suspendome;
Mechanical behavior;
Experimental investigation;
Numerical analysis;
Overall stability

1. Introduction

Nowadays, spatial structures employing steel, aluminum alloy, and glulam as primary materials, notably single-layer reticulated shells, have gained extensive utilization in contemporary public buildings. Ensuring the static stability of spatial structures constitutes an important aspect of structural design. To achieve a more comprehensive understanding of the static stability of single-layer reticulated shells, extensive investigations have been conducted through physical model testing. Ma et al. [1] conducted an experimental inquiry into a reticulated shell made of steel featuring bolt-ball joints, revealing that under the load of 22.43kN, instability occurred at the mid-span joint. Xiong et al. [2, 3] performed an experimental investigation on a reticulated shell connected by aluminum alloy gusset joints. Failure was observed in the rods near the mid-span node when subjected to a load of 99.7kN. For glulam reticulated shell, Lu et al. [4] carried out tests employing various rise-span ratios and bolt arrangement configurations. The structure exhibited an ultimate bearing capacity of approximately 5.50kN, with the failure mode primarily characterized by parallel-to-grain cracking in the compression zone of the glulam members.

Numerous studies have consistently demonstrated the inherent weaknesses in joint stiffness and overall stability within single-layer reticulated shells. To enhance the stability of reticulated shells, a novel structural form known as the suspendome structure has been developed [5]. The suspendome structure achieves higher stiffness and reduces structural deformation under similar loads by increasing cable-strut system within the single-layer reticulated shell. Many experts and scholars have conducted the static properties of the suspendome in detail through model tests, encompassing assessments of structural deformation under both design load and excessive load, as well as evaluating the impact of asymmetric loading on the structure [5-11]. However, there has been a scarcity of experiments conducted to investigate the stability of the suspendome structure. Zhang et al. [12] conducted tests on a suspendome structure, which experienced overall instability leading to pronounced collapse of the structure. The ultimate bearing capacity of the structure was determined to be 327.34kN. The basic profiles of experimental tests are shown in Table 1.

Table 1
Destructive tests of reticulated shells and suspendome

Structural form	Material	Dimension	Loading point	Ultimate load
Single-layer cylindrical reticulated shell [1]	Steel	Span: 5m×6m; Height: 1.25m	Single-point	22.4kN
Single-layer spherical reticulated shell [2, 3]	Aluminum alloy	Span: 8m; Height: 0.5m	Single-point	99.7kN
Single-layer spherical reticulated shell [4]	Glulam	Span: 4m; Height: 0.8m/0.4m	7-points	5.50kN
Suspendome [12]	Steel	Span: 9.3m;Height: 0.93m	442-points	327.34kN

To date, research on suspendome utilizing steel and aluminum alloy had indicated that the upper members of the structure predominantly experience compression. Taking into account the exceptional compressive capabilities of glulam, this paper innovatively applied it to the upper reticulated shell, thereby introducing a novel type of structure termed as the glulam suspendome. However, regarding the static properties and the overall stability of glulam suspendome, no experimental investigations have been conducted thus far.

In this study, the ultimate bearing capacity and the overall stability of glulam suspendome were studied through the destructive test of 13 hydraulic jacks. Based on the theoretical analysis of the instability of the glulam members, the failure mode of glulam suspendome was investigated. Using finite element software, the numerical model of the structure was established, while the parameter analysis of the structures was analyzed. Based on the ultimate bearing capacity of single-layer glulam reticulated shells, the ultimate bearing capacity improvement coefficient (k) of glulam suspendome was given. The test and numerical analysis results of the glulam suspendome have yielded satisfactory outcomes, providing valuable assistance to the structural design.

2. Experimental methods

2.1. Material test

As depicted in Fig. 1, tests were conducted to ascertain the parallel-to-grain compressive strength of the glulam material utilized in this study. TCT24 grade Douglas Fir glulam conforming to GB/T 50708-2012 [13] standard was used in the material test. The specimen was determined in accordance with ASTM

D143[14], while testing was conducted using a 100kN-capacity electronic universal testing machine. The test loading speed was controlled by displacement, with a specific speed of 0.3mm/min. The test results are shown in Table 2.

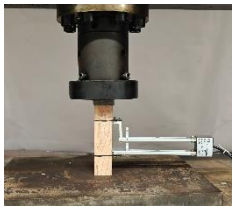

Fig. 1 Parallel-to-grain compressive test

Table 2
Test results of glulam material properties

Material properties (MPa)	Number of specimens	Average value $\bar{X}$	Standard deviation S	Coefficient of variation v
Parallel-to-grain elastic modulus	16	12254	1769	14.44%
Parallel-to-grain compressive strength		43.89	3.87	8.81%

2.2. Specimen design

Serving as the upper structure of the glulam suspendome, the single-layer glulam reticulated shell adopts the Kiewitt-6 structural configuration [15]. In accordance with the suggestions provided in technical specification [16] and relevant literature [17, 18], the design of glulam suspendome in this research entailed a span of 6m and a height of 1.2m, resulting a rise-span ratio of 0.2. The specimen was characterized by a strut height of 0.6 m, while the sag-span ratio was 1/400. The section size and material of each component were shown in Fig. 2.

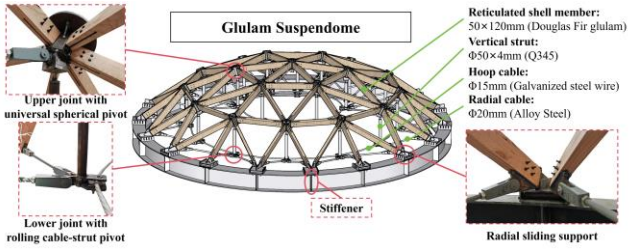

Fig. 2 Diagram and dimension of the glulam suspendome

2.3. Measurement layout

To investigate the mechanical properties of the glulam suspendome, it was essential to accurately measure the displacement of typical nodes, the strain of the members, and the tension of hoop cables. The specific measurement scheme followed the same approach as outlined in the reference [15].

2.4. Prestressed tension and loading scheme

In this research, the prestress ratio was 1:2[19]. LC1 was 4.5kN, while LC2 was 2.25kN. As depicted in Fig. 3, 13 hydraulic jacks were employed for synchronous loading in the destructive test.

The destructive test adopted the same loading method as the full-span loading, utilizing 13 hydraulic jacks to execute synchronous loading. At the beginning of the formal loading, the load was set to 0.1 times the predicted ultimate load (P_u) until the load reached 0.7 times P_u. When the load is 0.7 to 0.8 times Pu, the load for each stage was adjusted to 0.05 times Pu. Once the load reached 0.8 times P_u, a displacement-controlled loading method was adopted. According to ASTM D1761-12 [20], the loading speed was set at 0.9mm/min.

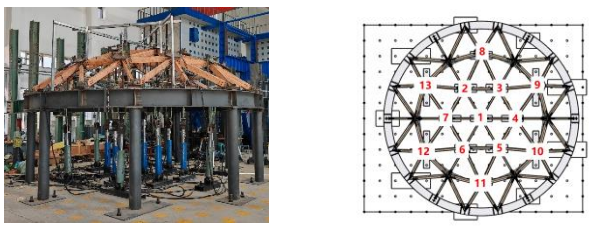

Fig. 3 Diagram of the formal loading in destructive loading

3. Destructive loading

3.1. Failure mode

The load-displacement curve of the 1st node is depicted in Fig. 4, along with the corresponding failure modes of the relevant members during the loading process. When the load reached 26kN, the first crack appeared in the first circumferential member, with the failure location observed in the 4th member. When loading to 52kN, the 55th member of the second main rib exhibited cracking near the bolts. Subsequently, when the load reached 72kN, the 58th member within the same circle sustained damage. The structural damage occurred in the upper reticulated shell of the glulam suspendome, while the cable-strut system remained undamaged.

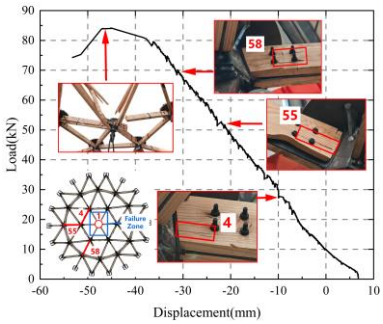

Fig. 4 Load-displacement curve

The ultimate load capacity of the structure was determined to be 84.17kN, with a total load reaching 1094.21kN (84.17kN×13). The displacement recorded at the 1st node reached -45.10mm. Upon reaching the ultimate load, the sound of crack within the glulam material became apparent. Parallel-to-grain cracking was observed in some of the main rib members adjacent to the 1st node. Concurrently, the 37th member experienced a fracture, roughly attributed to the member buckling. Meanwhile, other members adjacent to the 1st node exhibited instability along the weak axis. Members from the 37th to the 42nd rotated around the mid-span node. The structural failure mode was depicted in Fig. 5. Detailed buckling analysis was presented in Section 3.5.

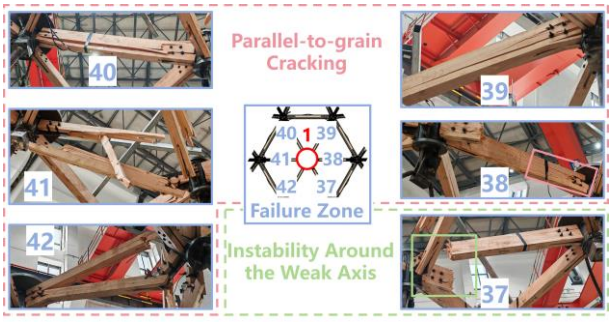

Fig. 5 Failure mode of glulam suspendome

3.2. Load-displacement curves

(1) Node displacement

As shown in Fig. 6a, the displacement of the 2nd, 3rd, 5th and 6th node were recorded as -42.9mm, -38.66mm, -31.65mm, and -35.95mm, respectively. The displacement of the nodes on the first ring exhibited a smaller magnitude compared to that of the 1st node, with a consistent change trend observed across these nodes. This observation suggested that the 13-point synchronous loading scheme effectively ensured symmetrical deformation of the structure.

As depicted in Fig. 6b, among the outer ring nodes of the glulam suspendome, the 15th node exhibited the largest displacement, measuring -24.55 mm. Since the main rib node of the second circle was not the loading point, its displacement was minimal. The displacement of the 8th, 10th, 14th and 16th node were recorded as -2.04mm, -13.14mm, -7.99mm, and -10.12mm, respectively.

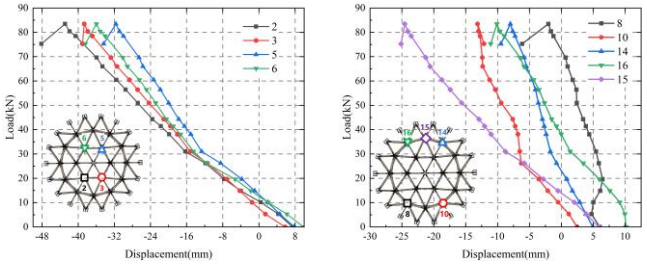

(a) 2, 3, 5, 6 (b) 8, 10, 14, 16, 15

Fig. 6 Node displacement

(2) Support displacement

As depicted in Fig. 7, all support displacements were observed to be radial outward. The displacement of the 35th support was the smallest, measuring 3.16mm. The displacements of 21st and 22nd supports were relatively close, measuring 7.91mm and 8.38mm, respectively.

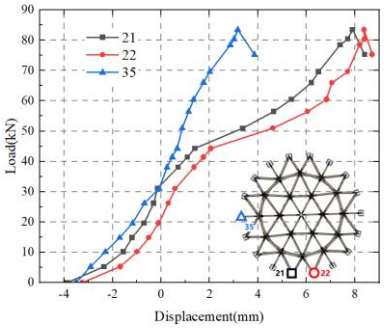

Fig. 7 Load-displacement curves in support

3.3. Cable tension curves

As shown in Fig. 8, the cable force of hoop cables exhibited a positive linear growth relationship with the load. When the structure experienced failure, LC1 measured 97.12kN, while LC2 was recorded as 24.69kN. LC1 was significantly larger than LC2 because nodes in the second circle transferred a greater load to the cable-strut system.

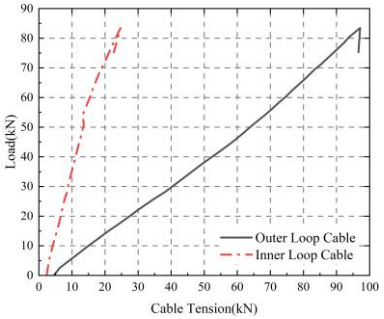

Fig. 8 Cable tension

3.4. Strain distribution curves

To further investigate the mechanical behavior of the glulam suspendome, representative members are selected to analyze.

(1) Reticulated shell member

The main rib members of reticulated shell were analyzed, and their load-strain curves were presented in Fig. 9. Throughout the loading process, the main rib members primarily experienced compression. As illustrated in Fig. 9b and d, the strain of the 39th and 37th member was recorded as -1388.95με and -2186.53με, respectively. The 39th and 37th members of the first circle exhibit the highest force, followed by the members of the second circle, and finally, the outermost ring members displayed the least force.

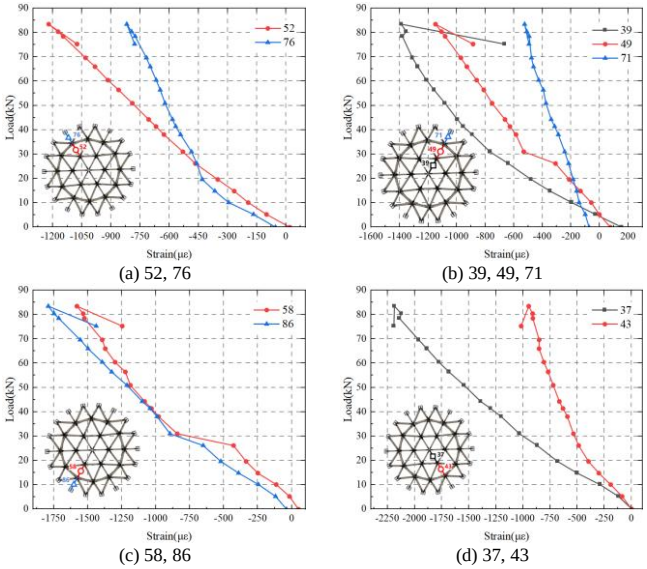

(a) 52, 76 (b) 39, 49, 71

(c) 58, 86 (d) 37, 43

Fig. 9 Load-strain curves in radial members

As depicted in Fig. 10, an analysis of the circumferential members of the reticulated shell was conducted. The members of the first ring experienced compression, while members of the second ring underwent strain. The strain of the 6th and 18th member at failure state was recorded as -930.64με, 189.57με, respectively.

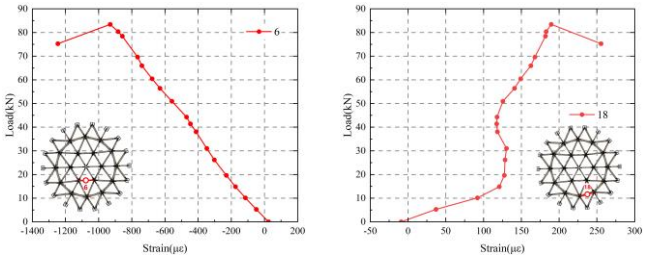

(a) 6 (b) 18

Fig. 10 Load-strain curves in circumferential members

As depicted in Fig. 11, an analysis of the diagonal members of the reticulated shell was conducted. Obviously, all diagonal members were subjected to compression, with the pressure trend of symmetric members exhibiting consistency. As shown in Fig. 11a, the strain of the 60th and 59th member was recorded as -1106.38με and -584.26με. As depicted in Fig. 11b, the strain of the 87th and 90th member approached -1800με, while the strain of the 88th and 89th member was close to -850με. The compressive strain of the 90th member was the largest, measured at -1865.93με.

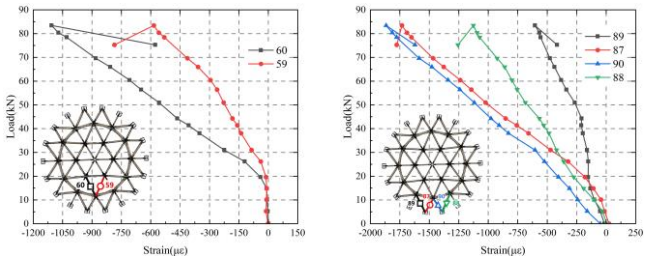

(a) 59, 60 (b) 89, 87, 90, 88

Fig. 11 Load-strain curves in diagonal members

(2) Vertical strut

As illustrated in Fig. 12, the struts of the glulam suspendome experienced compression during loading. The force on the 91st and 92nd struts was nearly identical, with their strain measuring close to -190με. Among the struts corresponding to the third circle nodes, the 97th strut exhibited the largest force, while the 98th strut had the smallest force. The maximum compressive strain was recorded at -242.23με.

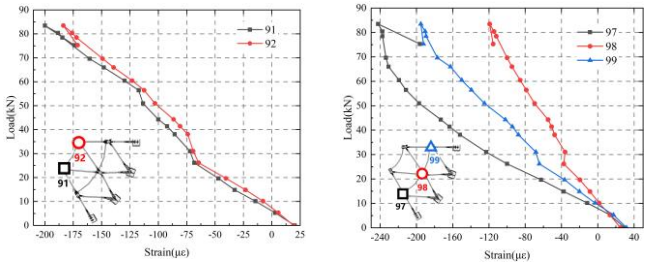

(a) 91, 92 (b) 97, 98, 99

Fig. 12 Load-strain curves in vertical struts

(3) Radial cable

The radial rods corresponding to the main rib members of the reticulated shell were analyzed, as shown in Fig. 13a. The strain of the 127th and 128th member was recorded as 408.35μεand 497.82με, respectively.

As shown in Fig. 13b, radial cables in the third circle were all tensioned, with a relatively consistent changing trend. Among them, the strain of the 151st rod was the largest, measuring 838.26με. The strain of the 161st and 164th rods was approximately 400με, while the strain of the 163rd rod was the smallest, measured at 85.62με.

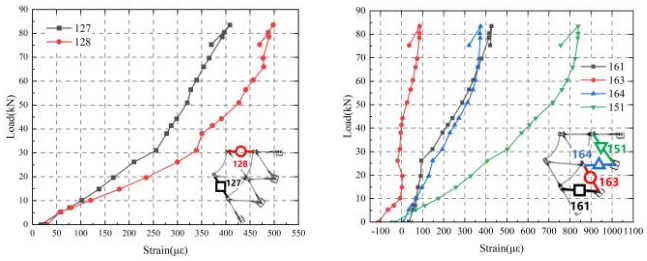

(a) 127, 128 (b) 161, 163, 164, 151

Fig. 13 Load-strain curves in radial cables

3.5. Analysis of the member buckling

As depicted in Fig. 14, an assessment was conducted to ascertain whether any glulam member became buckled by calculating the axial force of the main rib member. The approach to determining member instability is as follows: the axial force of the member should exceed the stable bearing capacity of a single member, calculated under standard hinged conditions at both ends, yet remain below the stable bearing capacity calculated assuming fixed joints at both ends. Additionally, the load-axial force curve of the member must exhibit a decreasing section after reaching its maximum value.

The stability bearing capacity can be calculated using the following formula [13]:

$$N = \varphi f_c A_0 \tag{1}$$

$$\varphi = \frac{1+(f_{cE}/f_c)}{1.8} - \sqrt{\left[\frac{1+(f_{cE}/f_c)}{1.8}\right]^2 - \frac{f_{cE}/f_c}{0.9}} \tag{2}$$

$$f_{cE} = \frac{0.47E}{(l_0/b)^2} \tag{3}$$

$$l_0 = k_l l \tag{4}$$

Where, f_c is the parallel-to-grain compressive strength of the glulam; A_0 is the area of the cross section of the member; φ is the stability reduction coefficient of axially loaded compression; E is the parallel-to-grain elastic modulus of the glulam; b is the width of the cross section; l_0 is the calculation length; k_l is the effective length factor, which is valued as 1.0 for the member which has hinge joint at both ends and is valued as 0.65 for the member which has fixed joint at both ends.

In this study, under conditions where both ends are hinged, the ultimate bearing capacity of the axial compression member is determined to be 109.14kN. Conversely, when both ends are fixed, the ultimate bearing capacity of the axial compression member is calculated to be 204.86kN. As illustrated in Fig. 14c and d, the axial forces acting on the 37th, 58th, and 86th members all adhere to the initial criterion of the judgment principle. Compared with the axial force of the 58th and 86th members, the axial force of the 37th member was greater. Therefore, it can be concluded that the 37th member experienced instability first, consequently leading to structural damage.

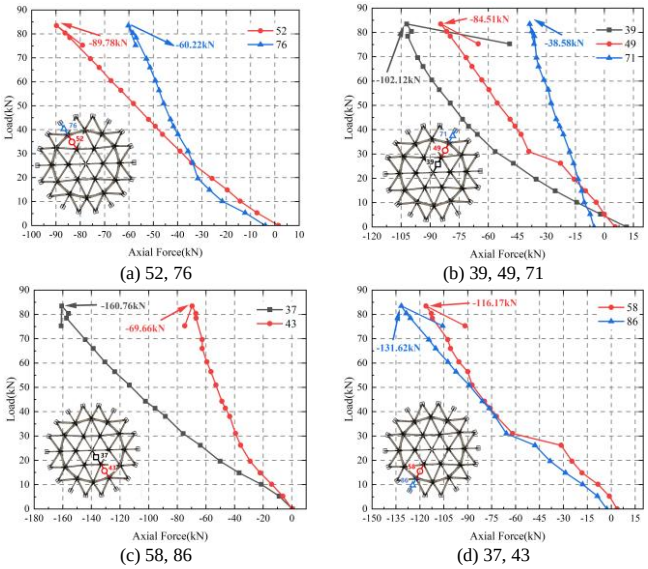

(a) 52, 76 (b) 39, 49, 71

(c) 58, 86 (d) 37, 43

Fig. 14 Load-Axial Force curves in radial members

In Fig. 15a, the failure mode of the aluminum reticulated shell depicted members near the loading point buckling around the weak axis, leading to the inclined failure of the structure [21]. As shown in Fig. 15b, it is evident from the literature [12] that the failure of the steel suspendome was attributed to the buckling of the local member. This phenomenon further highlights the importance of considering member stability and selecting appropriate slenderness ratios in the design of suspendome.

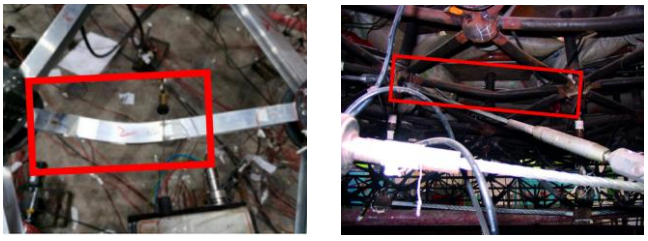

(a) Aluminum reticulated shell (b) Steel suspendome

Fig. 15 Failure mode of the members in the reticulated shell and suspendome

4. Parameter analysis

4.1. Validation of the FEM

The numerical model of the glulam suspendome was constructed using the ANSYS software. The glulam members were represented using BEAM188 elements. The vertical struts and radial cables were modeled using Link180 elements. Additionally, the hoop cables were represented using Link10 elements. The constraints applied to the finite element model included circumferential and vertical constraints on the outermost node. Prestress was applied to the structure by setting the initial strain of hoop cables.

As depicted in Fig. 16, the analysis focused on the 1st node to compare the test results with the results obtained from FEM. The structural deformation observed in the finite element model closely matched the experimental findings. The relative error of ultimate bearing capacity calculated by the FEM was 9.16%, compared with the experimental results.

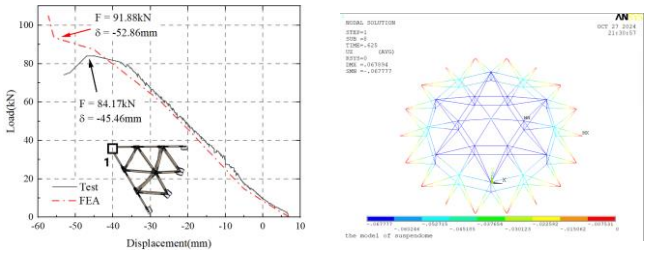

(a) Load-Displacement Curve (b) Node Displacement

Fig. 16 Comparison between FEM and test

4.2. Parameter analysis

In the parameter analysis, this paper selected the structural prestress, span and span-ratio, height of vertical struts, initial defections to analyze the overall stability of glulam suspendome. Table 3 showed the structural size and the section size of glulam member. The upper structure of glulam suspendome adopted K6-type reticulated shell, while each ring was built with a hoop cable. The prestress of the structure was applied by adjusting the cable force of hoop cables. Refer to relevant practical projects, the constraints were typically defined as radial sliding and circumferential constraints to reflect this design approach in FEM. Only the parallel-to-grain compressive strength is considered in this analysis, reflecting the primary loading condition of the glulam members.

The key parameters include the prestress ratio (the ratio of the cable force of each ring) and the prestress amplitude (the prestress of the outermost hoop cable). Fig. 17a showed the naming rules of the finite element model (FEM), while Fig. 17b showed the diagram of the FEM. The selection of parameters was as follows:

Span: 30m, 45m, 60m, 75m, 90m, 105m, 120m;

Span-Ratio (f/L): 1/5, 1/6, 1/8, 1/10, 1/12, 1/15;

Length of vertical struts(m): 2.0, 2.5, 3.0, 3.5, 4.0, 5.5, 6.0, 6.5, 7.0, 7.5;

Prestress Ratio: Ratio of the number of nodes corresponding to each loop cable;

Amplitude of prestress (kN): 90 (30m, 45m, 60m), 120 (75m, 90m, 105m, 120m);

Section of member: Vertical strut (φ219×7), Radial cable (φ80), Hoop cable (φ7×73).

Table 3
Structural parameters

Span (m)	30	45, 60	75, 90	105, 120
Section of glulam members (mm)	180×540	240×720	300×900	360×1080
Rings	5	7	9	11

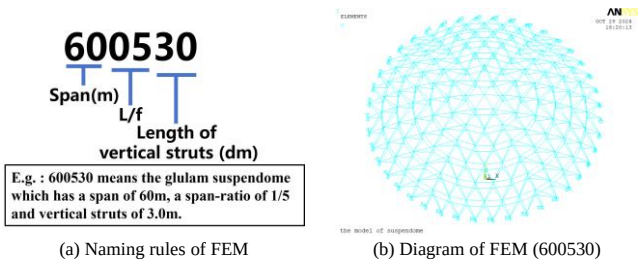

(a) Naming rules of FEM (b) Diagram of FEM (600530)

Fig. 17 Finite element model (FEM)

4.2.1. Prestress Amplitude and Initial Defection

Based on the glulam suspendome named “600530”, the initial prestress of the structure was changed to explore the influence of different prestresses on the overall stability of the structures. Concurrently, the influence of initial defects on the overall stability of glulam suspendome was studied by setting the initial defection values of different sizes.

As shown in Fig. 18a, different prestress amplitude had little effect on the ultimate bearing capacity of glulam suspendome. When the cable force of the outermost ring cable was 90kN (A), the ultimate bearing capacity of the structure was the maximum, which was 11.46kN/m^2. When the cable force of the outermost ring cable was increased to 1.4A, the ultimate bearing capacity of the structure was the smallest, which was 11.00kN/m^2. The ultimate bearing capacity of the structure was reduced by about 4.18%.

Damage to the upper reticulated shell occurred prior to the full activation of the load-bearing capacity of the lower cable-strut system. With greater prestress amplitude, the structural stiffness is enhanced, leading to reduced deformation under identical loading conditions. However, variations in prestress amplitude exert little influence on the stress distribution within the upper glulam members. As structural failures predominantly occur in the glulam components, often due to premature instability, the ultimate bearing capacity of the glulam suspendome is relatively insensitive to changes in prestress amplitude.

As depicted in Fig. 18b, different initial defections also had little influence on the ultimate bearing capacity of glulam suspendome. When the structure had no initial defection, the ultimate bearing capacity was 11.46kN/m^2. When the structural defection was L/100, the ultimate bearing capacity was 11.00kN/m^2, which was reduced by about 4.18%.

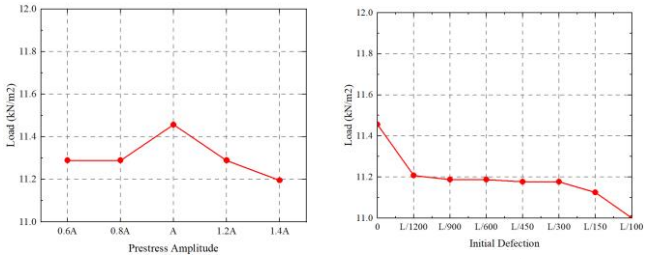

(a) Prestress Amplitude (b) Initial Defection

Fig. 18 Results of parameter analysis

4.2.2. Span, Span-ratio and Height of vertical struts

As shown in Fig. 19a, more than 200 cases of glulam suspendome with different span, span-ratio and length of struts were analyzed in order to explore the influence of structural span and span-ratio on structural stability bearing capacity. As shown in Fig. 19b, the ultimate bearing capacity of the structure decreased with the reduction of the span-ratio. Taking span-75m as an example, the ultimate bearing capacity of the structure was 125.31kN/m^2 when the span-ratio was 1/5. When the span-ratio is 1/15, the ultimate bearing capacity of the structure was 39.03kN/m^2, which decreased by 72.05%. With the decrease of the span-ratio, the force of the upper reticulated shell was more, which leaded to the easy destruction of glulam material.

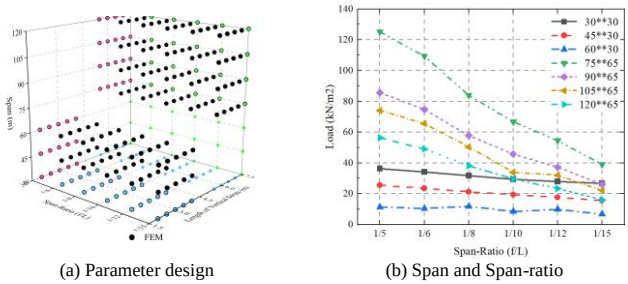

(a) Parameter design (b) Span and Span-ratio

Fig. 19 Span, Span-ratio and Height of vertical struts

As shown in Fig. 20a, as the length of the struts increased, the ultimate bearing capacity of the structure gradually increased. For example, when the length of the strut was 2.0m, the ultimate bearing capacity of the structure is the lowest, which was 22.78kN/m^2. When the strut length was 4.0m, the ultimate bearing capacity of the structure was the highest, which was 28.33kN/m^2, an increase of 24.36%. As shown in Fig. 20b, the ultimate bearing capacity of the

glulam suspendome with a span of more than 75m did not increase significantly with the increase of the length of the struts. This indicated that the overall stability of glulam suspendome with small span can be effectively improved by increasing the length of struts. However, for the structure with large span, it is necessary to increase the section size of the glulam members to improve the overall stability of the structure.

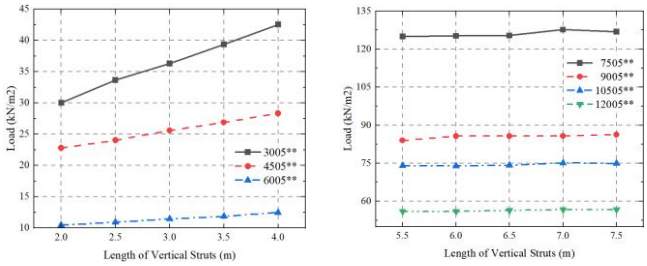

(a) 30m, 45m, 60m (b) 75m, 90m, 105m, 120m

Fig. 20 The length of vertical struts

4.3. Estimation of ultimate bearing capacity of glulam suspendome

At present, there were few theoretical studies on the overall stability performance of suspendome structure, and there was no corresponding calculation formula of ultimate bearing capacity. Based on the calculation of ultimate bearing capacity of single-layer glulam reticulated shells, the reinforcement factor "*k*" was proposed to estimate the ultimate bearing capacity of K6-type glulam suspendome. It is worth noting that the ultimate bearing capacity of K6 single-layer glulam reticulated shell was also calculated by FEM in Section 4.1.

$$k = \frac{\Lambda_{\text{suspendome}}}{\Lambda_{\text{shell}}} \tag{5}$$

$\Lambda_{suspendome}$ is the ultimate bearing capacity of glulam suspendome, kN/m^2; Λ_{shell} is the ultimate bearing capacity of the single-layer glulam reticulated shell corresponding to the suspendome, kN/m^2.

According to the parameter analysis in Section 4.2, the prestress and initial defection had little influence on the ultimate bearing capacity, while the span, span-ratio and strut length had great influence on the ultimate bearing capacity. Therefore, this paper carried out numerical simulation analysis on several groups of glulam suspendome with different spans, span-ratios and strut lengths, and put forward the growth coefficient table of K6-type structures (Table 4-10). The enhancement coefficient which was not given in the table can be calculated by interpolation. It can be inferred from the data that the smaller of the span-ratio and the longer the length of struts, the more obvious tension system can improve the overall stability of the structure.

Table 4
k- (Span= 30m)

Length of vertical struts (m)	Span-Ratio					
	1/5	1/6	1/8	1/10	1/12	1/15
2	1.75	1.82	1.91	2.03	2.24	2.83
2.5	1.97	2.01	2.15	2.29	2.57	3.29
3	2.12	2.20	2.38	2.54	2.84	3.66
3.5	2.30	2.40	2.58	2.78	3.12	4.06
4	2.48	2.59	2.79	3.03	3.39	4.45

Table 5
k- (Span= 45m)

Length of vertical struts (m)	Span-Ratio					
	1/5	1/6	1/8	1/10	1/12	1/15
2	1.27	1.27	1.30	1.38	1.45	1.67
2.5	1.34	1.34	1.37	1.46	1.55	1.81
3	1.42	1.41	1.44	1.53	1.64	1.94
3.5	1.50	1.49	1.50	1.60	1.73	2.06
4	1.57	1.55	1.57	1.66	1.82	2.20

Table 6
k- (Span= 60m)

Length of vertical struts (m)	Span-Ratio					
	1/5	1/6	1/8	1/10	1/12	1/15
2	1.24	1.23	1.28	1.31	1.43	1.52
2.5	1.29	1.28	1.34	1.38	1.52	1.64
3	1.35	1.34	1.41	1.45	1.61	1.76
3.5	1.40	1.40	1.47	1.52	1.70	1.87
4	1.48	1.46	1.52	1.59	1.78	1.99

Table 7
k- (Span= 75m)

Length of vertical struts (m)	Span-Ratio					
	1/5	1/6	1/8	1/10	1/12	1/15
5.5	1.10	1.09	1.18	1.23	1.29	1.33
6	1.10	1.11	1.18	1.24	1.30	1.34
6.5	1.10	1.10	1.17	1.24	1.30	1.34
7	1.12	1.11	1.18	1.24	1.31	1.35
7.5	1.12	1.12	1.19	1.25	1.31	1.36

Table 8
k- (Span= 90m)

Length of vertical struts (m)	Span-Ratio					
	1/5	1/6	1/8	1/10	1/12	1/15
5.5	1.12	1.13	1.23	1.34	1.41	1.45
6	1.14	1.14	1.24	1.33	1.41	1.46
6.5	1.14	1.14	1.24	1.33	1.42	1.46
7	1.14	1.14	1.25	1.34	1.42	1.47
7.5	1.15	1.16	1.25	1.34	1.42	1.49

Table 9
k- (Span= 105m)

Length of vertical struts (m)	Span-Ratio					
	1/5	1/6	1/8	1/10	1/12	1/15
5.5	1.15	1.18	1.27	1.40	1.52	1.51
6	1.15	1.18	1.33	1.42	1.54	1.51
6.5	1.16	1.19	1.33	1.42	1.55	1.52
7	1.17	1.19	1.34	1.46	1.56	1.52
7.5	1.17	1.20	1.34	1.47	1.56	1.52

Table 10
k- (Span= 120m)

Length of vertical struts (m)	Span-Ratio					
	1/5	1/6	1/8	1/10	1/12	1/15
5.5	1.17	1.20	1.42	1.56	1.64	1.64
6	1.17	1.20	1.42	1.57	1.68	1.65
6.5	1.18	1.20	1.42	1.58	1.69	1.65
7	1.18	1.20	1.42	1.60	1.71	1.66
7.5	1.18	1.22	1.43	1.61	1.73	1.67

5. Conclusions

In this study, a novel type of glulam suspendome is proposed. A destructive test with 13-point synchronous loading is conducted on a structural model with a span of 6m and a height of 1.2m. Based on the analysis of structural failure mode, load-displacement curves and load-strain curves, the mechanical properties of glulam suspendome are investigated. Based on the analysis of structural parameters, the method of estimating the ultimate bearing capacity of the structure and the improvement coefficient (k) are proposed. The following conclusions are drawn:

(1) In the destructive test, the failure load recorded at each loading point is 84.17kN, resulting in a total load received by the glulam suspendome of 1094.21kN (84.17kN×13). The failure mode of the structure involved instability around the weak axis of the member near the mid-span node, along with member fracture. The displacement of the mid-span node is the largest, measuring -47.10mm. The compressive strain of the main rib member of the first layer is the largest, measured at -2186.53με (-160.76kN). This suggests that the importance of considering member stability and selecting appropriate slenderness ratios in the design of the glulam suspendome.

(2) In the destructive test, the second ring members in the reticulated shell are subjected to tension. Consequently, the corresponding position of the vertical struts experiences greater pressure, resulting in higher tension in the outer ring radial rods. This observation indicates that the load of the glulam suspendome is primarily transmitted downwards to the cable-strut system through the outer ring nodes. In the design of the glulam suspendome, the load dispersion effect of the outer cable-strut system should be taken into consideration.

(3) The parameter analysis of more than 200 finite element models showed that prestress and initial defections had little influence on the overall stability of glulam suspendome. The geometrical dimensions of the structure, such as the span-ratio and the length of vertical struts, had a great influence on the overall stability of glulam suspendome. It is worth noting that when the span of the structure is greater than 75m, the ultimate bearing capacity of the structure cannot be effectively improved by increasing the length of the struts.

(4) By comparing the ultimate bearing capacity of single-layer glulam reticulated shell and glulam suspendome of the same size, the reinforcement factor "k" of glulam suspendome was given. The results showed that the smaller of the span-ratio and the longer the length of the strut, the more obvious tension system can improve the overall stability of the structure.

Acknowledgements

This work was supported by the Hebei Natural Science Foundation (No. E2020402074).

References

[1] Ma H, Fan F, Wen P, Zhang H, Shen S. Experimental and numerical studies on a single-layer cylindrical reticulated shell with semi-rigid joints. Thin-Walled Structures. 2015;86:1-9.
[2] Xiong Z, Guo X, Luo Y, Zhu S. Elasto-plastic stability of single-layer reticulated shells with aluminium alloy gusset joints. Thin-Walled Structures. 2017;115:163-75.
[3] Xiong Z, Guo X, Luo Y, Zhu S, Liu Y. Experimental and numerical studies on single-layer reticulated shells with aluminium alloy gusset joints. Thin-Walled Structures. 2017;118:124-36.
[4] Lu B, Ye Y, Ji Y, Lu W, Pan X, Huang Y et al. Investigations on the critical load of mid-span Kiewitt-type single-layer timber reticulated shells considering the effect of joint stiffness. Structures. 2024;63:106423.
[5] Kawaguchi M, Abe M, Tatemichi IJJ-IAfS, Structures S. Design, tests and realization of suspen-dome system. 1999;40:179-92.
[6] Guo J, Dong S, Yuan X. Research on static property of suspen-dome structure under heap load. Advanced Steel Construction. 2012;8:137-52.
[7] Nie G, Zhi X, Fan F, Shen S. Study of the tension formation and static test of a suspendome for Dalian Gymnasium. China civil engineering journal. 2012;45:1-10.
[8] Chen ZH, Yan RZ, Wang XD, Liu HB, Xiao X. EXPERIMENTAL RESEARCHES OF A SUSPEN-DOME STRUCTURE WITH ROLLING CABLE-STRUT JOINTS. ADVANCED STEEL CONSTRUCTION. 2015;11:15-38.
[9] Xue S, Lu Z, Li X, Liu R, Zhao Z, Jing H et al. Experimental and numerical investigations on the influence of center-hung scoreboard on dynamic characteristics of suspend-dome structure. Journal of Building Engineering. 2022;57:104787.
[10] Xue S, Wang Z, Li X, Liu R, Lu Z, Jing H et al. Model test study on static performance of rib-patterned small rise-span ratio suspend-dome structure. Structures. 2022;43:1615-28.
[11] Yan RZ, Zhu MH, Liu T, Liu JQ, Chen ZH. EFFECT OF RANDOM PRE-STRESSED FRICTION LOSS ON THE PERFORMANCE OF A SUSPEN-DOME STRUCTURE. ADVANCED STEEL CONSTRUCTION. 2022;18:465-78.
[12] Zhang A, Liu X, Wang D, Wei W, Huang D, Wu L et al. Static experimental study on the model of the suspend-dome of the badminton gymnasium for 2008 Olympic Games. Journal of Building Structures. 2007;28:58-67.
[13] GB/T 50708-2012. Technical code of glued laminated timber structures. China Architecture and Building Press. Beijing; 2012
[14] ASTM D143-2014. Standard test methods for small clear specimens of timber. United States; 2014
[15] Liu H, Zhao J, Zhao J, Chen Z, Zhao S, Yang S. Experimental study on the mechanical behavior of glulam suspendome considering the influence of prestressing. Journal of Building Engineering. 2024;95:110180.
[16] JGJ7-2010. Technical specification for space frame structures. China Building Industry Press. Beijing; 2010
[17] Pan DH, Girhammar UA. Influence of Geometrical Parameters on Behaviour of Reticulated Timber Domes. International Journal of Space Structures. 2003;18:105-21.
[18] Pan D, Girhammar UA. Effect of Ring Beam Stiffness on Behaviour of Reticulated Timber Domes. International Journal of Space Structures. 2005;20:143-60.
[19] Kang W, Chen Z, Lam H-F, Zuo C. Analysis and design of the general and outmost-ring stiffened suspen-dome structures. Engineering Structures. 2003;25:1685-95.
[20] ASTM D1761-12. Test Methods for Mechanical Fasteners in Wood. United States; 2012
[21] Sun GJ, Xiao S, Wu JZ, Yu SF, Wei MY, Qin J et al. Study on the static stability of aluminum alloy single-layer spherical reticulated shell. JOURNAL OF BUILDING ENGINEERING. 2024;84.